Repeatability Assessment of Intravascular Polarimetry in Patients

Martin Villiger, *Member, IEEE*, Kenichiro Otsuka, Antonios Karanasos, Pallavi Doradla, Jian Ren, Norman Lippok, Milen Shishkov, Joost Daemen, Roberto Diletti, Robert-Jan van Geuns, Felix Zijlstra, Jouke Dijkstra, Gijs van Soest, Evelyn Regar, Seemantini K. Nadkarni, and Brett E. Bouma

***Abstract*— Intravascular polarimetry with polarization sensitive optical frequency domain imaging (PS-OFDI) measures polarization properties of the vessel wall and offers characterization of coronary atherosclerotic lesions beyond the cross-sectional image of arterial microstructure available to conventional OFDI. A previous study of intravascular polarimetry in cadaveric human coronary arteries found that tissue birefringence and depolarization provide valuable insight into key features of atherosclerotic plaques. In addition to various tissue components, catheter and sample motion can also influence the polarization of near infrared light as used by PS-OFDI. This paper aimed to evaluate the robustness and repeatability of imaging tissue birefringence and depolarization in a clinical setting. 30 patients scheduled for percutaneous coronary intervention at the Erasmus Medical Center underwent repeated PS-OFDI pullback imaging, using commercial imaging catheters in combination with a custom-built PS-OFDI console. We identified 274 matching cross sections among the repeat pullbacks to evaluate the reproducibility of the conventional backscatter intensity, the birefringence, and the depolarization signals at each spatial location across the vessel wall. Bland–Altman analysis revealed best agreement for the birefringence measurements, followed by backscatter intensity, and depolarization, when limiting the analysis to areas of meaningful birefringence. Pearson correlation analysis confirmed highest correlation for birefringence (0.86), preceding backscatter intensity (0.83), and depolarization (0.78). Our results demonstrate that intravascular polarimetry generates robust maps of tissue birefringence and depolarization in a clinical setting. This outcome motivates the use of intravascular polarimetry for future clinical studies that investigate polarization properties of arterial atherosclerosis.**

***Index Terms*— Endoscopy, evaluation and performance, heart, optical imaging, optical coherence tomography, polarimetry, validation, vessels.**

Manuscript received November 24, 2017; revised March 4, 2018; accepted March 5, 2018. Date of publication March 21, 2018; date of current version June 30, 2018. This work was supported in part by the National Institutes of Health under Grant P41EB-015903 and Grant R01HL-119065, and in part by Terumo Corporation. The work of K. Otsuka was supported in part by the Japan Heart Foundation and in part by the Bayer Yakuhin Research Grant Abroad. *(Corresponding author: Martin Villiger.)*

M. Villiger, K. Otsuka, P. Doradla, J. Ren, N. Lippok, M. Shishkov, and S. K. Nadkarni are with the Wellman Center for Photomedicine, Massachusetts General Hospital, Harvard Medical School, Boston, MA 02114 USA (e-mail: mvilliger@mgh.harvard.edu; kotsuka@mgh.harvard.edu; pdoradla@mgh.harvard.edu; jren@mgh.harvard.edu; nlippok@mgh.harvard.edu; shishkov@helix.mgh.harvard.edu; snadkarni@mgh.harvard.edu).

A. Karanasos was with the Department of Interventional Cardiology, Thoraxcenter, Erasmus Medical Center, Rotterdam, The Netherlands. He now is with the First Department of Cardiology, Hippokration Hospital, University of Athens, Athens, Greece (e-mail: akaranasos@hotmail.com).

J. Daemen, R. Diletti, R.-J. van Geuns, F. Zijlstra, and G. van Soest are with the Department of Interventional Cardiology, Thoraxcenter, Erasmus Medical Center, Rotterdam, The Netherlands (e-mail: j.daemen@erasmusmc.nl; r.diletti@erasmusmc.nl; r.vangeuns@erasmusmc.nl; f.zijlstra.1@erasmusmc.nl; g.vansoest@erasmusmc.nl).

J. Dijkstra is with the Department of Radiology, Leiden University Medical Center, Leiden, The Netherlands (e-mail: j.dijkstra@lumc.nl).

E. Regar was with the Department of Interventional Cardiology, Thoraxcenter, Erasmus Medical Center, Rotterdam, The Netherlands. She now is with the Heart Center, University Hospital Zurich, Zürich, Switzerland (e-mail: evelyn.regar@usz.ch).

B. E. Bouma is with the Wellman Center for Photomedicine, Massachusetts General Hospital, Harvard Medical School, Boston, MA 02114 USA, and also with the Institute for Medical Engineering and Science, Massachusetts Institute of Technology, Cambridge, MA 02142 USA (e-mail: bouma@mgh.harvard.edu).

Color versions of one or more of the figures in this paper are available online at http://ieeexplore.ieee.org.

Digital Object Identifier 10.1109/TMI.2018.2815979

I. Introduction

INTRAVASCULAR optical coherence tomography (OCT) and optical frequency domain imaging (OFDI), a second-generation implementation of OCT, currently offer the highest spatial resolution for invasive coronary imaging. Visualizing the detailed plaque microstructure has helped to advance our understanding of the pathogenesis of coronary artery disease [1], [2] and has offered new strategies to guiding percutaneous coronary interventions in clinical practice [3], [4]. The high spatial resolution has enabled investigation of fibrous cap morphology in plaque disruption [5]–[7] and erosions [8], the two major pathways to acute coronary events. It also offered insight into macrophage accumulation [9], [10], considered an important contributor to plaque instability. Despite the merits of contemporary intravascular imaging, there remains a need for improved imaging methods to furnish novel insights into the mechanisms of thrombotic complications, and to evaluate the effects of therapeutic interventions. Combining OCT with the superior imaging depth of intravascular ultrasound (IVUS) would enable evaluation of plaque burden together with microstructural details [11]. Fluorescence, from endogenous origin or injectable imaging probes offers an interesting avenue to complement OCT and enhance plaque characterization [12]–[16], but requires custom multimodal imaging catheters. We have previously reported on

intravascular polarimetry with polarization sensitive (PS) OFDI as a promising strategy to dissect individual aspects of plaque morphology that is compatible with commercial intravascular imaging catheters [17]. The microscopic structure and organization of the arterial wall influence the polarization of near infrared light [18]. Collagen and arterial smooth muscle cells exhibit birefringence, an optical property that results in a differential delay, or retardation, between light polarized parallel to the tissue fibrillar components versus light having a perpendicular polarization. Intravascular PS-OFDI of cadaveric human coronary arteries showed elevated birefringence in regions of fibrous, collagen-rich tissue, and in the tunica media due to a high number of smooth muscle cells [17]. Plaque regions rich in lipid, cholesterol crystals, and macrophages displayed depolarization, corresponding to the randomization of the scattered polarization states. Together with maps of tissue birefringence and depolarization, PS-OFDI generates conventional cross-sectional images of backscatter intensity, revealing the subsurface microstructure, and offers detailed characterization of atherosclerotic tissue morphology.

Intravascular polarimetry was enabled by advances in reconstructing tissue birefringence and depolarization and by mitigating artifacts that are induced by the imaging system and the rotating catheter [19]–[22]. The polarization of the near infrared light used for PS-OFDI is impacted when propagating through the catheter and is influenced by catheter and sample motion that are unavoidable in a clinical setting. To evaluate the robustness of imaging polarization features under such conditions and validate the ability to perform meaningful polarimetry in humans, we performed a pilot study in 30 patients [23]. Here we assessed the repeatability of quantifying tissue birefringence and depolarization by inspecting matching cross-sections of repeat pullbacks, and used the repeatability of structural imaging with conventional backscatter intensity for comparison.

II. Methods

A. Study Population

This first in man pilot study of intravascular polarimetry enrolled 30 non-consecutive patients undergoing percutaneous coronary intervention between December 2014 and July 2015 at the Erasmus Medical Center in Rotterdam. All procedures were performed as previously reported [24], and in accordance with local and federal regulations and the Declaration of Helsinki. The study protocol was approved by the Ethics Committee of Erasmus Medical Center and all patients gave written informed consent.

B. Polarization Sensitive Optical Frequency Domain Imaging

Commercial intravascular catheters (FastView, Terumo) were used in conjunction with a custom-built state-of-the-art OFDI system. Similar to commercial instruments, the imaging system operated at a center wavelength of 1300 nm with a wavelength scanning range of 110 nm, corresponding to a radial resolution of 9.4 μm in tissue, assuming a refractive index of 1.34. The catheter was pulled back at a speed of 20 mm/s, and images were acquired at a rate of 100 frames/s, each consisting of 1024 radial scans, during injection of non-ionic contrast solution at a rate of 1–3 mL/s. In each patient, at least two PS-OFDI pullbacks were performed, either in the native coronary artery (N = 9) or after the procedure (N = 15). In a subset of patients (N = 6) both pre- and post-procedural pullbacks were acquired.

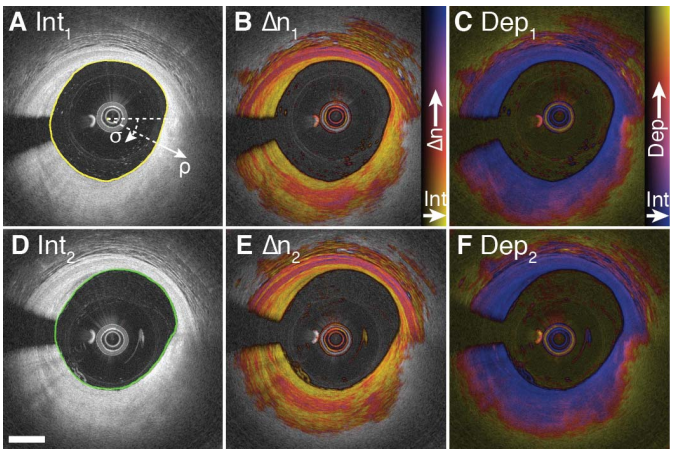

Fig. 1. PS-OFDI of an atherosclerotic plaque measured in repeat pullbacks. (A, D) Intensity of the backscatter signal showing subsurface plaque morphology in conventional logarithmic gray scale. The yellow and green lines indicate the lumen segmentations. Panel A indicates the angular position σ and depth in the tissue ρ with respect to the center of the lumen. (B, E) Display of birefringence in color hue and reflection signal in brightness. Birefringence is only shown in regions of low depolarization, converting to gray-scale backscatter signal in areas of high depolarization. The color range encodes birefringence from 0 to 2.2×10^{-3}. (C, F) Display of depolarization in color hue and backscatter signal in brightness. The color range encodes depolarization from 0 to 0.5. Scale bar: 1 mm.

Intravascular polarimetry was previously described [17]. In short, the imaging system was equipped with a polarization diverse receiver to determine the polarization state of the light scattered by the tissue, and an electro-optic polarization modulator to vary the polarization state of the light illuminating the vessel wall between consecutive radial scans. Polarimetric analysis was performed offline with spectral binning [22] to reconstruct maps of tissue birefringence and depolarization. Birefringence is the unitless ratio of retardation and the distance over which it was accrued. It corresponds to the difference, Δn, of the refractive index experienced by two orthogonal polarization states, aligned with the fast and slow optic axis of the birefringent tissue. As a measure of tissue depolarization, we computed the complement to 1 of the degree of polarization. Depolarization indicates increasing randomization of the detected polarization states in the range 0–1. Figure 1 illustrates the reconstructed birefringence ($\Delta n_{1,2}$) and depolarization ($Dep_{1,2}$) of a plaque with mostly fibrous intimal tissue and some dispersed lipid together with the conventional log-scaled backscatter intensity ($Int_{1,2}$), imaged during two consecutive pullbacks.

C. Data Analysis

Repeat pullbacks were reviewed to identify matching segments with acceptable contrast and a smooth lumen, excluding

regions of stents, plaque rupture, detached thrombus, or poor image quality. We excluded the data sets of 3 patients due to a lack of suitable segments. One patient had two coronaries imaged, and in total we further analyzed 9 pairs of repeat pullbacks in native coronary arteries, 13 pairs in treated vessels, and 6 pairs from patients that underwent both pre and post procedural PS-OFDI. Using visual hallmarks in the conventional backscatter images, such as side-branches, plaque morphology, and calcifications, we identified closely matching cross-sections, blinded to the polarization signals, and visually adjusted their relative angular orientation using custom viewing software written in Matlab (Mathworks, Natick, MA, USA). Consecutive matching sections were spaced by at least 10 frames (2 mm). We identified a total of 274 matching sections, 241 resulting from immediate repeat pullbacks in native (115) or treated vessels (126), and 33 matching sections that were acquired pre and post procedure. At least two cross-sections were identified in each artery. Lumen contour segmentation was performed in the matching sections with QCU-CMS viewing software (Leiden University Medical Center, Leiden, The Netherlands), as visualized in Figure 1.

Imported into Matlab, the contours enabled unwrapping of the lumen about its apparent center with an elastic transformation method to recover the cross-sections in cylindrical coordinates, ρ, the depth within the vessel wall, and σ, the angular position along the lumen, as illustrated in Figures 1 and 2A. For spatially detailed comparison, the relative angular position between matching sections was refined by translating the second unfolded cross-section by $\Delta\sigma$ along σ to reduce the normalized mismatch between the backscatter intensity signals:

$$\min_{\Delta\sigma} \frac{\sum_{\rho,\sigma} (Int_1(\rho,\sigma) - Int_2(\rho,\sigma+\Delta\sigma))^2}{\sqrt{\sum_{\rho,\sigma} Int_1(\rho,\sigma)^2}\sqrt{\sum_{\rho,\sigma} Int_2(\rho,\sigma)^2}} \quad (1)$$

where the sums were taken only over points with a signal at least 15 dB above the noise floor in both sections. This masked signal from peri-adventitial tissue and the regions shadowed by the guide-wire. The correction step is visualized in Figure 2C, D with the color-coded overlay of the originally unwrapped and the corrected backscatter intensity images. The resulting effect on the birefringence maps is visualized in Figure 2E, F. After refining the angular alignment, all sections were remapped to Cartesian coordinates, onto the lumen contour of the first cross-section, offering close spatial matching (Figure 2G, H). To assess the repeatability of the conventional backscatter and the polarimetric signals, we compared the cross-sections by averaging the signal within circular regions of interest (*ROI*) of diameter D, translated across the entire images in steps of $D/2$ in an automated, rigid pattern. *ROI*-positions that had more than half of the pixels with a depolarization below a threshold, $Dep \leq DepTh$, were excluded from correlation analysis, shown in Figures 2I-K. The depolarization threshold limits the analysis depth within the vessel wall by masking peri-adventitial tissue and the guide-wire shadow, as well as lipid-rich tissue regions, as visualized in Figures 2G, H.

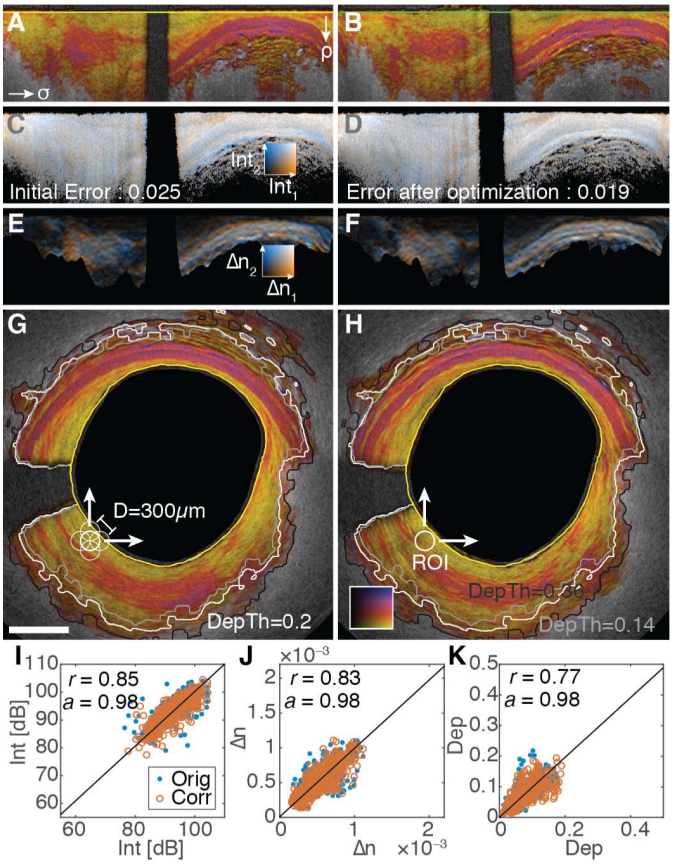

Fig. 2. Refinement of spatial co-registration and correlation analysis. (A, B) Unwrapped sections of Figure 1. (C) Color-coded overlay of the two backscatter intensity images visualizing original relative error. Areas with a signal <15 dB above the noise floor are masked. (D) Adjusting the relative angular offset of the second section by −11.38° reduces the error. (E, F) Corresponding overlay of the birefringence images. Areas with a depolarization >0.2 are masked. (G, H) Co-registered sections mapped back into Cartesian coordinates onto the lumen of the first section. White and light and dark gray lines indicate transition of depolarization signal below 0.2, 0.14, and 0.36, respectively. Scale bar: 1 mm. (I-K) Correlation plots for backscatter intensity (I), birefringence (J), and depolarization (K) for the original (blue dots) and corrected (orange circles) sections, with a depolarization threshold of 0.2. *r* indicates the Pearson correlation coefficient, and *a* the slope of the Deming regression. Black lines show Deming regression.

D. Statistical Methods

We computed Pearson correlation coefficients between the *ROI*-values of individual matching sections, or the compound *ROI*-values of all (or a subset of the) sections. We also performed Deming regression, which finds the best linear fit by reducing the total least square error, assuming equal errors in both correlated variables. A paired Student's t-test was used to compare the correlation coefficients of the three signal types. Two one-sided t-tests were used to evaluate equivalence of the Deming regression with a slope of one. Significance was set at 5 %.

Bland-Altman plots of the *ROI*-values were created as an alternative assessment of the agreement between the repeat measurements. The 95 % limits of agreement (LoA) were estimated using the 2.5th and 97.5th percentile of the difference signals. All statistical analysis was performed with Matlab.

TABLE I
PARAMETERS EXTRACTED FROM BLAND-ALTMAN ANALYSIS

	Intensity	Δn	Dep
Median difference	−0.181 dB	1.37×10^{-6}	-1.40×10^{-4}
LoA(–)	6.14 dB	0.25×10^{-3}	0.057
LoA(+)	6.35 dB	0.24×10^{-3}	0.054
Median / LoA(±) [%]	2.007	0.176	0.015
Median of average	90.32 dB	0.60×10^{-3}	0.081
Range: 2.5th to 97.5th percentile	18.66 dB	0.83×10^{-3}	0.128
Contrast: Range / 2×LoA(±)	1.49	1.68	1.16

Dep: Depolarization. LoA(–) is the 2.5th to 50th percentile and LoA(+) the 50th to 97.5th percentile of the difference signal. LoA(±) is their mean.

III. RESULTS

A. Bland-Altman Analysis

To assess the overall agreement between repeat pullbacks for the conventional backscatter image and the polarimetric signals, we matched 274 cross-sections of varying lesion type, but excluding regions of stents, plaque rupture, or detached thrombus, and generated Bland-Altman plots, analyzed with an *ROI* diameter of 300 μm. The depolarization threshold was set to $DepTh = 0.2$, which has the effect of restricting the analysis mostly to the vessel wall and excluded signal from deeper tissue regions and peri-adventitial layers that typically feature higher depolarization. Applying a depolarization threshold is critical for the analysis of birefringence, because the randomization of the polarization states underlying increased depolarization precludes the reconstruction of meaningful birefringence in these areas.

To account for the large number of data points, we generated 2D histograms, binning the difference between the mean signals of corresponding *ROIs* against their average, as displayed in Figure 3. Table 1 summarizes the computed parameters. Because the difference signal was not strictly normally distributed, we used the 2.5th and 97.5th percentile of the difference signal to compute the LoAs. The polarimetric signals resulted in median differences smaller than 2 % of the mean LoA. For the intensity signal, the mean difference corresponds to 2 % of the LoA. To interpret the LoAs, we compared them with the range (2.5th to 97.5th percentile) of the average signal, corresponding to the aspect ratio of the Bland-Altman plot, and offering a measure of the practically available contrast in the images. The larger the variation of the average signal, the higher is the dynamic range of the signal encountered in the measured vessels. And the smaller the LoAs, the more signal levels can be reliably differentiated within this dynamic range. Birefringence presented the highest ratio, suggesting a relatively higher dynamic range or smaller LoA than for the backscatter intensity or depolarization signals in the analyzed tissue regions.

B. Pearson Correlation Analysis

We also performed Pearson correlation analysis on the compounded data points of all matching cross-sections. Figure 4A displays the resulting correlation coefficients for all three signals. Birefringence had the highest correlation ($r = 0.856$, 95 % confidence interval (CI) 0.854–0.858), followed by intensity ($r = 0.833$, 95 % CI 0.831–0.835), and depolarization

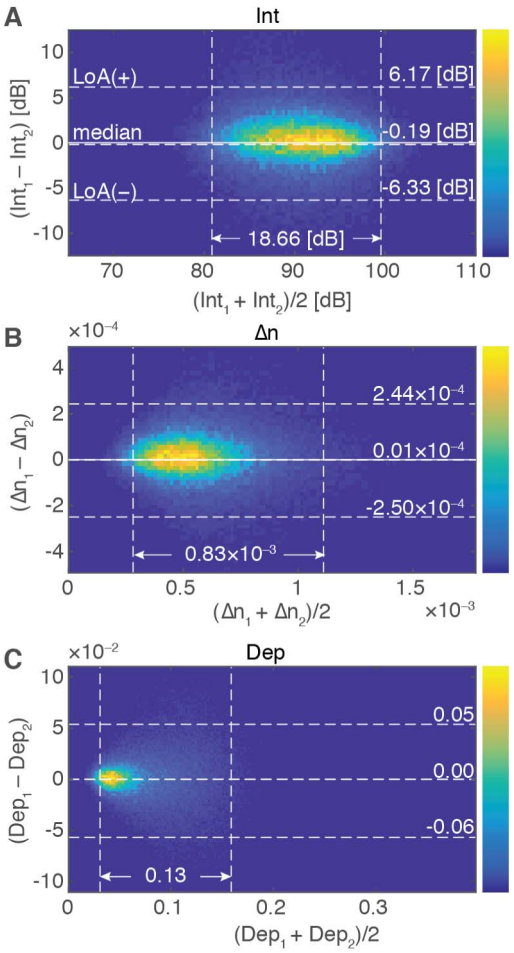

Fig. 3. Bland-Altman Analysis for (A) backscatter intensity (Int), (B) birefringence Δn, and (C) depolarization (Dep), in areas with a depolarization ≤0.2. All panels show mean offsets and the limits of agreement (LoA), as well as the 95 % confidence interval on the mean average signal.

resulted in the poorest correlation ($r = 0.780$, 95 % CI 0.777–0.783). The same analysis was applied to the cross-sections acquired by immediate repeat pullbacks, and compared to the few cases where the first pullback was acquired in the native coronary artery before angioplasty, followed by imaging after the procedure. The necessary repeated deployment of the imaging catheter resulted in lower correlations.

In addition to compounding all cross-sections, we also retrieved the correlation coefficients for the individual sections, and displayed their means and standard deviations in Figure 4B. In this analysis the intensity achieved slightly higher mean correlation than the birefringence, but without statistical significance ($p = 0.108$), when compounding all cross-sections. The correlation of the intensity and the depolarization signal differed significantly ($p < 0.001$). For the immediate repeat measurements, intensity differed with statistical significance from both birefringence and depolarization ($p = 0.0079$ and $p < 0.001$, respectively). The differences between immediate repeat measurements and imaging pre and post procedure were also significant ($p < 0.001$). Table 2 summarizes the correlation results.

TABLE II
PEARSON CORRELATION ANALYSIS

	ALL (N=274)			REPEAT (N=241)			PRE/POST (N=33)		
Compound	*Int*	*Δn*	*Dep*	*Int*	*Δn*	*Dep*	*Int*	*Δn*	*Dep*
Corr. Coeff.	0.833	0.856	0.780	0.849	0.870	0.792	0.701	0.760	0.694
95% CI	0.831–0.835	0.854–0.858	0.777–0.783	0.847–0.851	0.868–0.871	0.789–0.795	0.690–0.712	0.751–0.769	0.683–0.705
Individual									
Corr. Coeff.	0.822	0.806	0.794	0.845	0.819	0.809	0.656	0.713	0.690
Standard Deviation	0.137	0.137	0.107	0.104	0.130	0.095	0.218	0.150	0.132

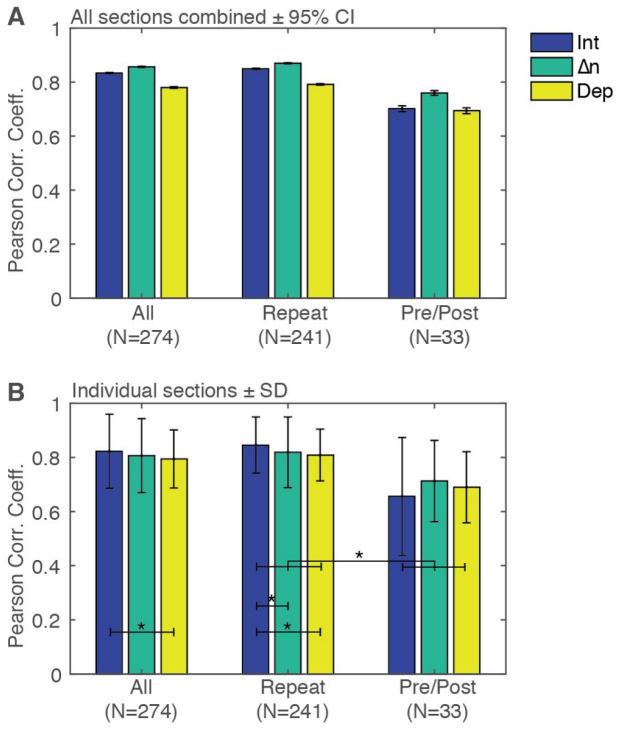

Fig. 4. Pearson correlation analysis. (A) Correlation of all compounded cross-sections (All), cross-sections imaged with immediate repeat pull-backs (Repeat), and cross sections that were measured pre and post therapy (Pre/Post). Error-bars indicate 95 % confidence intervals on the upper and lower bounds. (B) Correlation of individual cross-sections for the same categories as in (A). Error bars indicate ± standard deviation (SD). $* p < 0.001$.

Figure 5A illustrates the distribution of the correlation coefficient of the three signals. Although high correlation coefficients were most frequent for the intensity signal, it also resulted in a few very poor correlations. In comparison, the polarimetric signals distributed more narrowly around high correlation values. In Figure 5B the distribution of the slope of the Deming regression is visualized. All signals centered around a unitary slope. Using two one sided t-tests we minimized the equivalence interval at a significance level of 95 % and obtained intervals of 0.09, 0.06, and 0.03 for the correlation slope of the intensity, birefringence, and depolarization, respectively. These intervals confirm the more narrow distribution of the polarimetric signals compared to the intensity.

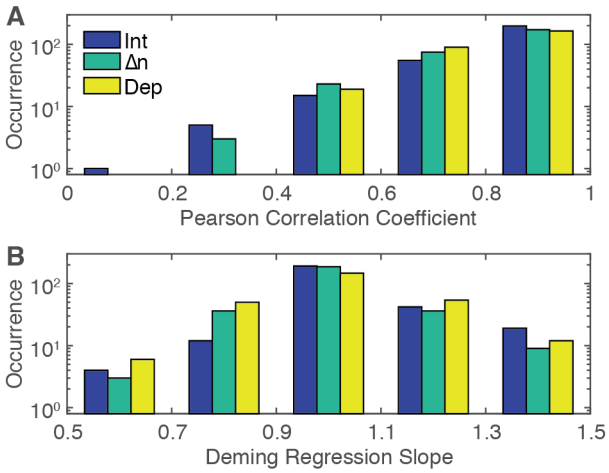

Fig. 5. Pearson correlation analysis and Deming regression. A) Histogram of the Pearson correlation coefficients for all 274 cross-sections. B) Histogram of the Deming regression slope.

C. Dependence on ROI Diameter and Depolarization Threshold

In the previous analysis, the *ROI* diameter was kept at 300 μm and the depolarization threshold at $DepTh = 0.20$. Figure 6 displays the correlation coefficients of the compounded 274 cross-sections for varying *ROI* diameters and depolarization thresholds. For the birefringence signal, the correlation improved substantially with increasing *ROI* diameter, whereas the intensity signal proved less sensitive to this parameter. Below a diameter of 200 μm, the intensity resulted in a better correlation than the birefringence. The depolarization exhibits a more modest increase with growing *ROI* size and plateaus at around 300 μm.

Higher depolarization corresponds to increased randomness in the measured polarization states, which limits the reconstruction of meaningful birefringence. Accordingly, in response to an increased depolarization threshold, the correlation of the birefringence rapidly degrades, and improves for a smaller depolarization threshold. In contrast, both the intensity and the depolarization signal benefit of the inclusion of the deeper lying tissue regions and achieve higher correlations. Figure 6 also shows the mean maximum depth analyzed on all the sections as a function of the depolarization threshold.

To demonstrate the significance of the reported correlations, we introduced an artificial angular offset of 30° to the unfolded

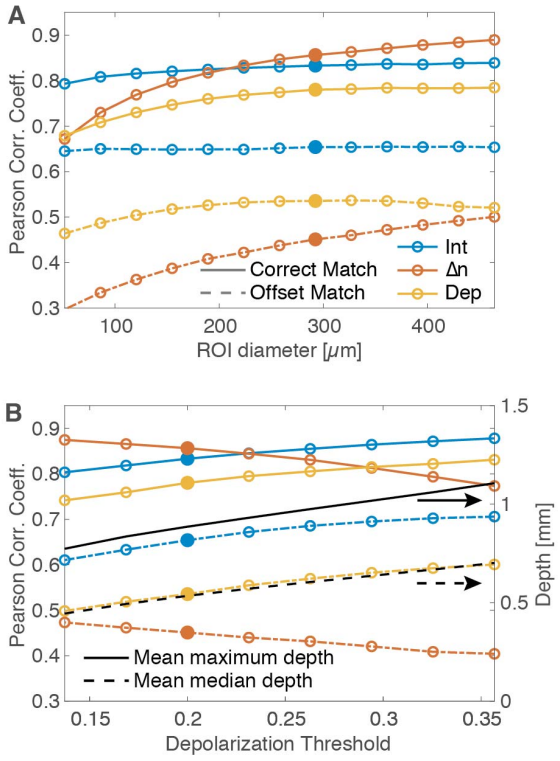

Fig. 6. Pearson correlation analysis for different *ROI* diameters and depolarization thresholds. (A) Influence of *ROI* diameter at a depolarization threshold $DepTh = 0.20$. (B) Influence of the depolarization threshold at an *ROI* diameter of 300 μm. The black line indicates the mean of the maximum depth analyzed in each section as a function of the depolarization threshold. Full lines correspond to correctly matched sections, and dashed lines to sections that were purposely offset by 30° in the angular direction. Full circles indicate points corresponding to previous analysis.

second cross-sections. This drastically reduced the correlations of the polarimetric signals, and to a lesser extent as well of the backscatter intensity signal.

IV. Discussion

Polarization sensitive OFDI measures the polarization state of the light scattered by the tissue, with the polarization of the illumination alternating between radial scans. Observation of how the measured polarization states vary along depth and between neighboring pixel locations permits reconstruction of maps of tissue birefringence and depolarization. This approach offers additional contrast that complements the structural information available from the backscatter intensity, and may offer a more detailed characterization of atherosclerotic plaques. Figure 7 shows an example of a mixed plaque in the right coronary artery of a 64-year-old woman who presented with unstable angina. The increased birefringence facilitates the identification of the tunica media. Compared to the fibrous area of the plaque discussed in Figures 1 and 2, the majority of the plaque area in this cross-section exhibits very low birefringence, which could imply that it corresponds to a healing thrombus rather than a collagen-rich fibrous lesion. The increased depolarization from 11 to 3 o'clock suggests the presence of lipid, macrophages, and cholesterol crystals.

To enable the further investigation and interpretation of these polarization signatures in clinical studies, we first strove to confirm and validate the reliability and robustness of these polarization metrics when evaluated in a clinical setting. Overall, we found an excellent agreement between the birefringence maps of spatially matched cross-sections acquired during repeat pullbacks. Repeat birefringence measurements agreed even better than conventional backscatter images, when analyzed with a low depolarization threshold and sufficiently large *ROI*. This result may arise from the quantitative nature of birefringence that reduces its LoAs, as well as from the rich birefringence contrast in the vessel wall, which results in a wider signal range compared to the backscatter signal and enhances the correlation.

The intensity signal varies in proportion to the power of the light illuminating the vessel wall. It depends on variations in the transmission through the catheter, and upon the reference signal in the interferometer. Even though two images acquired with a different overall intensity may visualize the same spatial features, their direct correlation would be skewed. We are unaware of any previous study assessing the repeatability of backscatter intensity for intravascular imaging, and our results may provide helpful parameters for the development of robust intensity-based segmentation algorithms and image processing routines.

Because the polarization of light transmitted through optical fibers is very sensitive to fiber motion, this raised additional concerns for the robustness of intravascular polarimetry [20]. The present results demonstrate that the reconstructed quantitative polarization metrics are insensitive to fiber motion and are more resilient to variations in the amplitude of the detected signal than the intensity images. Inspecting the individual cross-sections with poorest intensity correlations revealed that many exhibit slight shadowing artifacts due to suboptimal flushing, without, however, significantly altering the recovered polarization signatures.

The limited dynamic range of the backscatter signal from within the vessel wall further inhibits the correlation of the intensity signal. Backscatter appears quite uniform in the intimal layer and fibrous plaques, and is just slightly reduced in the tunica media. Only the hypoechoic signal of calcifications and lipid-rich regions result in a larger modulation of the scattering amplitude. In consequence, the intensity signal mostly visualizes large-scale features and is less sensitive to detailed spatial co-registration of matching cross-sections, as confirmed by its independence of the *ROI* diameter.

In comparison, birefringence varies substantially within the vessel wall. It is pronounced in the tunica media and elevated within areas of fibrous tissue, defining clearly demarcated zones of distinct birefringence levels on a scale smaller than most intensity features. Accordingly, the birefringence signal offers a wider dynamic range and is the most sensitive to precise spatial co-registration. Despite careful matching and the automated angular orientation correction, cardiac movement impeded exact co-registration of cross-sections acquired in live patients, and intrinsically limited its accuracy. The discrepancies identified in between repeat measurements may not arise solely from measurement inconsistencies, but may result from the limited spatial matching. We attribute the reduced correlation of cross-sections imaged before

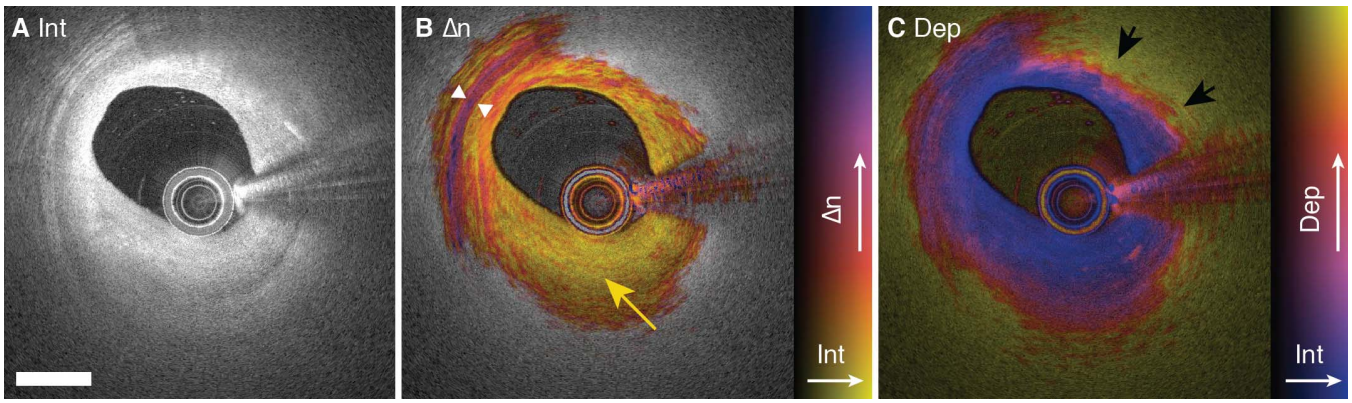

Fig. 7. PS-OFDI in the right coronary artery of a 64-year-old woman. A) Backscatter intensity, B) birefringence and intensity overlay, C) depolarization and intensity overlay. Birefringence is increased in the tunica media (white arrow heads), but otherwise the majority of this lesion appears lowly birefringent (yellow arrow). Depolarization highlights lipid and possible macrophages and cholesterol crystals (black arrows). Scale bar: 1 mm.

and after angioplasty to less accurate co-registration due to the altered position of the catheter within the vessel. Poor birefringence correlation of individual sections imaged during immediate repeat pullbacks associated with imperfect spatial co-registration in an angular region of those cross-sections.

Depolarization highlights areas of lipid, macrophages, and cholesterol crystals, but generally offers the fewest spatial features, and resulted in the poorest correlation. Applying the depolarization threshold artificially limited its dynamic range, and our depolarization metric did not take into account its dependence on the effective polarization state of the light incident on the tissue [25].

Using a higher depolarization threshold improves the dynamic ranges of the intensity and the depolarization signal by adding *ROI*s with lower intensity and higher depolarization, respectively, and enhances the observed correlations of these signals. The resulting LoA in the Bland-Altman analysis would increase more modestly than the dynamic range and improve their contrast ratio. Because the birefringence in regions of increased depolarization is meaningless and random, raising the depolarization threshold compromises the correlation of the birefringence signal between repeat measurements. It would increase the LoAs in the Bland-Altman analysis and reduce the contrast ratio.

As visualized in Fig. 2, even the lowest evaluated depolarization threshold (0.14) includes the entire vessel wall in areas with minimal disease, where the tri-layered structure of the artery is apparent in the intensity image. However, the OFDI signal does not penetrate the full thickness of lipid-rich plaques. The depolarization remains low within the fibrous cap and then rapidly increases within the underlying lipid-pool, from where no meaningful birefringence can be extracted. Increasing the depolarization threshold thus primarily adds peri-adventitial tissue areas and deeper located lipid-rich areas to the analysis, without, however, adding diagnostically relevant information. In our previous study of intravascular polarimetry [17], we employed the same depolarization threshold of 0.2 as in the current study. The mean maximum depth for this threshold (0.88 mm) corresponds closely to previous reports of mean wall thickness of normal coronary arteries (0.8 mm and 0.71 mm, respectively) [26], [27]. The mean median depth (0.53mm), because influenced by the shallower analysis depth in lipid-rich lesions areas, is smaller than this value, although the effective vessel wall is thicker in diseased arteries.

The strong dependence of the birefringence correlation on the *ROI* size agrees with the presence of more spatial features with a scale comparable to the *ROI* size than in the intensity or depolarization images. A larger *ROI* reduces the error due to inaccurate spatial matching and improves the resulting correlation. Because the intensity and depolarization signals vary more gradually, their correlation depends less on the *ROI* size.

Of note, the size of all employed *ROIs* sufficed to effectively average the speckle that is typically present in the intensity signal.

Limitations of this work include the manual identification of matching cross-sections, and residual matching errors due to imprecise lumen segmentation and cardiac motion. Normal looking vessel wall and atherosclerotic lesions were not differentiated and both used identically for analysis of repeatability.

V. Conclusion

This study demonstrates that intravascular polarimetry with PS-OFDI generates reliable and robust maps of tissue polarization properties. Tissue birefringence showed better correlation between repeat measurements than the conventional backscatter intensity signal, when restricting the analysis to areas of modest depolarization. This result underlines the quantitative nature of the birefringence metric and the wide range of birefringence levels encountered in atherosclerotic arterial vessels. Depolarization showed weaker but satisfying correlation. Combined, these results support the future use of intravascular polarimetry for clinical studies investigating birefringence and depolarization signatures across a spectrum of clinical presentations.

References

[1] T. Yonetsu, B. E. Bouma, K. Kato, J. G. Fujimoto, and I.-K. Jang, "Optical coherence tomography," *Circulation J.*, vol. 77, no. 8, pp. 1933–1940, 2013.

[2] G. J. Tearney *et al.*, "Consensus standards for acquisition, measurement, and reporting of intravascular optical coherence tomography studies: A report from the international working group for intravascular optical coherence tomography standardization and validation," *J. Amer. College Cardiol.*, vol. 59, no. 12, pp. 1058–1072, Mar. 2012.

[3] F. Prati *et al.*, "Angiography alone versus angiography plus optical coherence tomography to guide decision-making during percutaneous coronary intervention: The centro per la Lotta contro l'infarto-optimisation of percutaneous coronary intervention (CLI-OPCI) study," *EuroIntervention*, vol. 8, no. 7, pp. 823–829, Nov. 2012.

[4] Z. A. Ali *et al.*, "Optical coherence tomography compared with intravascular ultrasound and with angiography to guide coronary stent implantation (ILUMIEN III: OPTIMIZE PCI): A randomised controlled trial," *Lancet*, vol. 388, no. 10060, pp. 2618–2628, Nov. 2016.

[5] S. Takarada *et al.*, "Effect of statin therapy on coronary fibrous-cap thickness in patients with acute coronary syndrome: Assessment by optical coherence tomography study," *Atherosclerosis*, vol. 202, no. 2, pp. 491–497, Feb. 2009.

[6] T. Yonetsu *et al.*, "*In vivo* critical fibrous cap thickness for rupture-prone coronary plaques assessed by optical coherence tomography," *Eur. Heart J.*, vol. 32, no. 10, pp. 1251–1259, May 2011.

[7] S. Uemura *et al.*, "Thin-cap fibroatheroma and microchannel findings in optical coherence tomography correlate with subsequent progression of coronary atheromatous plaques," *Eur. Heart J.*, vol. 33, no. 1, pp. 78–85, Jan. 2012.

[8] H. Jia *et al.*, "*In vivo* diagnosis of plaque erosion and calcified nodule in patients with acute coronary syndrome by intravascular optical coherence tomography," *J. Amer. College Cardiol*, vol. 62, no. 19, pp. 1748–1758, Nov. 2013.

[9] J. E. Phipps *et al.*, "Macrophages and intravascular OCT bright spots: A quantitative study," *JACC, Cardiovascular Imag.*, vol. 8, no. 1, pp. 63–72, Jan. 2015.

[10] L. Di Vito *et al.*, "Identification and quantification of macrophage presence in coronary atherosclerotic plaques by optical coherence tomography," *Eur. Heart J. Cardiovascular Imag.*, vol. 16, no. 7, pp. 807–813, Jul. 2015.

[11] J. Li *et al.*, "Integrated IVUS-OCT for real-time imaging of coronary atherosclerosis," *Cardiovascular Imag.*, vol. 7, no. 1, pp. 101–103, Jan. 2014.

[12] H. Yoo *et al.*, "Intra-arterial catheter for simultaneous microstructural and molecular imaging *in vivo*," *Nature Med.*, vol. 17, no. 12, pp. 1680–1684, Dec. 2011.

[13] G. J. Ughi *et al.*, "Clinical characterization of coronary atherosclerosis with dual-modality OCT and near-infrared autofluorescence imaging," *JACC, Cardiovascular Imag.*, vol. 9, pp. 1304–1314, Nov. 2016.

[14] J. W. Verjans *et al.*, "Targeted near-infrared fluorescence imaging of atherosclerosis: Clinical and intracoronary evaluation of indocyanine green," *JACC, Cardiovascular Imag.*, vol. 9, no. 9, pp. 1087–1095, Sep. 2016.

[15] S. Kim *et al.*, "Intracoronary dual-modal optical coherence tomography-near-infrared fluorescence structural–molecular imaging with a clinical dose of indocyanine green for the assessment of high-risk plaques and stent-associated inflammation in a beating coronary artery," *Eur. Heart J.*, vol. 37, no. 37, pp. 2833–2844, Oct. 2016.

[16] J. B. Kim *et al.*, "Intravascular optical imaging of high-risk plaques *in vivo* by targeting macrophage mannose receptors," *Sci. Rep.*, vol. 6, Mar. 2016, Art. no. 22608.

[17] M. Villiger *et al.*, "Coronary plaque microstructure and composition modify optical polarization: A new endogenous contrast mechanism for optical frequency domain imaging," *JACC, Cardiovascular Imag.*, E-pub ahead of print, doi: 10.1016/j.jcmg.2017.09.023.

[18] S. K. Nadkarni *et al.*, "Measurement of collagen and smooth muscle cell content in atherosclerotic plaques using polarization-sensitive optical coherence tomography," *J. Amer College Cardiol.*, vol. 49, no. 13, pp. 1474–1481, Apr. 2007.

[19] M. Villiger, E. Z. Zhang, S. Nadkarni, W.-Y. Oh, B. E. Bouma, and B. J. Vakoc, "Artifacts in polarization-sensitive optical coherence tomography caused by polarization mode dispersion," *Opt. Lett.*, vol. 38, no. 6, pp. 923–925, Mar. 2013.

[20] M. C. Pierce *et al.*, "Effects of sample arm motion in endoscopic polarization-sensitive optical coherence tomography," *Opt. Exp.*, vol. 13, no. 15, pp. 5739–5749, Jul. 2005.

[21] E. Z. Zhang and B. J. Vakoc, "Polarimetry noise in fiber-based optical coherence tomography instrumentation," *Opt. Exp.*, vol. 19, no. 18, pp. 16830–16842, Aug. 2011.

[22] M. Villiger, E. Z. Zhang, S. K. Nadkarni, W.-Y. Oh, B. J. Vakoc, and B. E. Bouma, "Spectral binning for mitigation of polarization mode dispersion artifacts in catheter-based optical frequency domain imaging," *Opt. Exp.*, vol. 21, no. 14, pp. 16353–16369, Jul. 2013.

[23] J. N. van der Sijde, A. Karanasos, M. Villiger, B. E. Bouma, and E. Regar, "First-in-man assessment of plaque rupture by polarization-sensitive optical frequency domain imaging *in vivo*," *Eur. Heart J.*, vol. 37, no. 24, p. 1932, Jun. 2016.

[24] J. N. van der Sijde *et al.*, "Safety of optical coherence tomography in daily practice: A comparison with intravascular ultrasound," *Eur. Heart J. Cardiovascular Imag.*, vol. 18, no. 4, pp. 467–474, Apr. 2017.

[25] N. Lippok *et al.*, "Depolarization signatures map gold nanorods within biological tissue," *Nature Photon.*, vol. 11, no. 9, pp. 583–588, Jul. 2017.

[26] D. D. McPherson *et al.*, "Variable morphology of coronary atherosclerosis: Characterization of atherosclerotic plaque and residual arterial lumen size and shape by epicardial echocardiography," *J. Amer. College Cardiol.*, vol. 19, no. 3, pp. 593–599, Mar. 1992.

[27] C. J. van Andel, P. V. Pistecky, and C. Borst, "Mechanical properties of porcine and human arteries: Implications for coronary anastomotic connectors," *Ann. Thoracic Surg.*, vol. 76, no. 1, pp. 58–64, Jul. 2003.